

StegaFFD: Privacy-Preserving Face Forgery Detection via Fine-Grained Steganographic Domain Lifting

Guoqing Ma^{1,2†}, Xun Lin^{3†}, Hui Ma⁴, Ajian Liu^{1,4}, Yizhong Liu³, Wenzhong Tang³, Shan Yu^{1,2}, Chenqi Kong⁵ and Yi Yu^{5*}

¹Institute of Automation, Chinese Academy of Sciences, Beijing 100190, China.

²School of Future Technology, University of Chinese Academy of Sciences, Beijing 100049, China.

³Beihang University, Beijing 100191, China.

⁴Macau University of Science and Technology, Macau SAR 999078, China.

⁵ROSE Lab, School of EEE, Nanyang Technological University, Nanyang Avenue 639798, Singapore.

*Corresponding author(s). E-mail(s): yu.yi@ntu.edu.sg;

†These authors contributed equally to this work.

Abstract

Most existing Face Forgery Detection (FFD) models assume access to raw face images. In practice, under a client-server framework, private facial data may be intercepted during transmission or leaked by untrusted servers. Previous privacy protection approaches, such as anonymization, encryption, or distortion, partly mitigate leakage but often introduce severe semantic distortion, making images appear obviously protected. This alerts attackers, provoking more aggressive strategies and turning the process into a cat-and-mouse game. Moreover, these methods heavily manipulate image contents, introducing degradation or artifacts that may confuse FFD models, which rely on extremely subtle forgery traces. Inspired by advances in image steganography, which enable high-fidelity hiding and recovery, we propose a **Steganography-based Face Forgery Detection** framework (StegaFFD) to protect privacy without raising suspicion. StegaFFD hides facial images within natural cover images and

directly conducts forgery detection in the steganographic domain. However, the hidden forgery-specific features are extremely subtle and interfered with by cover semantics, posing significant challenges. To address this, we propose Low-Frequency-Aware Decomposition (LFAD) and Spatial-Frequency Differential Attention (SFDA), which suppress interference from low-frequency cover semantics and enhance hidden facial feature perception. Furthermore, we introduce Steganographic Domain Alignment (SDA) to align the representations of hidden faces with those of their raw counterparts, enhancing the model's ability to perceive subtle facial cues in the steganographic domain. Extensive experiments on seven FFD datasets demonstrate that StegaFFD achieves strong imperceptibility, avoids raising attackers' suspicion, and better preserves FFD accuracy compared to existing facial privacy protection methods.

Keywords: steganography, image hiding, face forgery detection, privacy protection, differential attention, feature lifting

1 Introduction

Compared with fingerprints, irises, and voiceprints, the face image is more intuitive, has richer information, a lower acquisition cost, and can be used in a non-contact manner. Therefore, it has been extensively used in identity authentication and identification services [1–4]. However, face images are easy to forge. In recent years, with the rise of face forgery technology and tools like FaceApp, FaceSwap, and DeepFaceLab [5], even non-professionals can manipulate face images, leading to widespread fake faces online. This poses significant security risks in areas such as justice, politics, reputation, and criminal investigations [6–8], necessitating face forgery detection (FFD) techniques [9–13]. In recent years, significant attention has been paid to face forgery detection, with models based on physiological signal analysis [14], intrinsic features [15], and deep learning [16–18]. Deep learning-based models, in particular, have shown promise in effectively distinguishing real faces from face-forgery ones.

Despite the impressive performance of deep neural networks, there are increasing concerns about security issues [19–27] associated with artificial intelligence, especially with the client-server architecture. Among these security issues, the protection of users' privacy remains a severe challenge [28]. From a legal and ethical perspective, people's facial images must be rigorously protected, ensuring the security and privacy of these images during their storage, transmission, and analysis processes [29] in client-server scenes. Institutions managing facial data have adopted methods such as data anonymization or pseudonymization [30] to mitigate the risk of data leakage. However, real-world scenarios indicate that these methods are not robust against re-identification attacks [31].

As illustrated in Fig. 1 (a), there is a risk of leakage, especially during the transmission of images from a client to a server [32]. Although techniques like

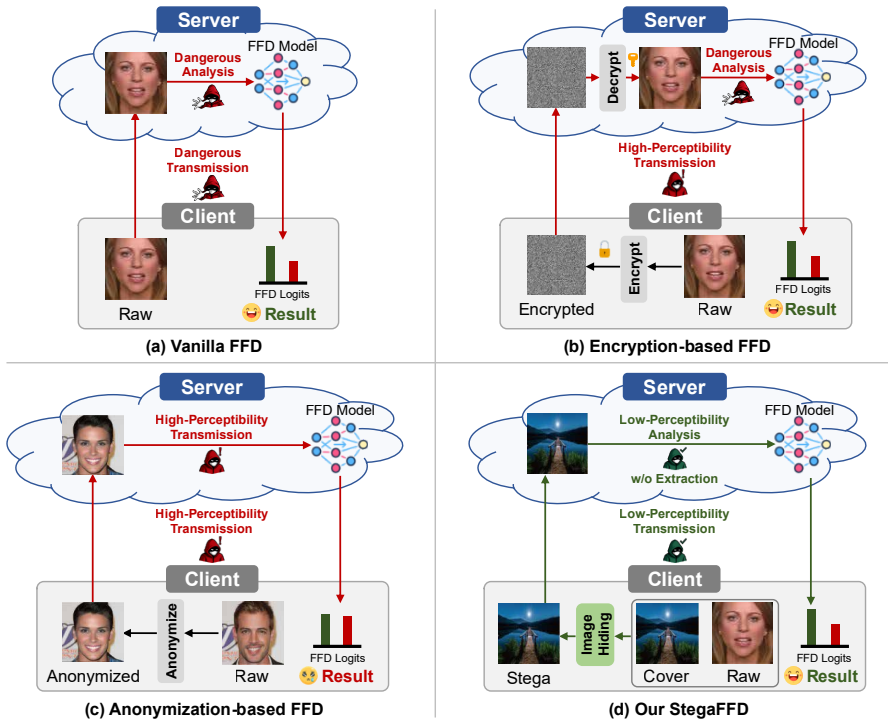


Fig. 1 Different client-server frameworks for FFD, including (a) vanilla, (b) encryption-based, (c) anonymization-based, and (d) the proposed StegaFFD framework. Our StegaFFD makes the attacker fail to notice the existence of facial images.

non-homomorphic image encryption can prevent image leakage during transmission, as shown in Fig. 1 (b), they are not robust to attacks from malicious servers [33]. Once an attacker controls the server through system vulnerabilities or embedded malicious backdoors (as a third-party server provider), the decrypted images on the server-side are also at risk of being captured. Face anonymization methodologies [34] induce synthetic characteristics in genuine images, consequently degrading the detection efficacy of face forgery detection algorithms, as shown in Fig. 1 (c). We position StegaFFD as a covert client-server FFD framework that avoids revealing facial content during transmission and requires no decryption on the server, as shown in Fig. 1 (d). It is noteworthy that the server returns to the client the “logit indicating whether the face image is forged.” This process does not pose a privacy leakage issue. Since attackers are likely to assume that our input image is a normal image without faces, it is difficult for them to discern the meaning of this logit.

Currently, most image privacy enhancement technologies focus on the training phase, for instance, by enabling different institutions to collaboratively train models without the direct exchange of image data through federated learning [35, 36]. These methods effectively enhance the privacy protection

of training data. Some studies focus on protecting images after deployment through distortion-based [33, 37, 38] methods to modify detailed information of the original images. Although these methods somewhat protect image privacy, attackers can easily notice that the transmitted images are facial images. To further enhance security, recent works propose encoding-based [39, 40] and homomorphic-encryption-based [41, 42] methods to protect facial images. However, these methods significantly alter the distribution of the images, easily alerting attackers to the fact that the images are protected by specific techniques, thus falling into a cat-and-mouse game of encryption and decryption. Among these methods, methods based on homomorphic encryption are time-consuming, making them impractical for many real-world applications, as shown in Table 1.

Recent progress in deep image hiding (DIH) networks [43–45], which are proposed to conceal a secret image within a cover image for covert image transmission, has inspired us to propose a novel framework to perform Face Steganographic Domain Analysis (StegaFFD) based on DIH. As shown in Fig. 1 (d), StegaFFD hides a facial image within a natural photo, allowing for direct FFD in the steganographic domain without the image extraction and decryption on the server-side. However, conducting FFD directly on stego images is challenging. The facial-specific features crucial for FFD are intrinsically weak, and their signal becomes even fainter in the steganographic domain. Meanwhile, the dominant information from the cover image acts as pervasive noise, effectively drowning out these critical but feeble cues.

Stego images carry most scene semantics in low-frequency bands, whereas DIH typically embeds secrets in relatively higher-frequency details to remain imperceptible [44, 46, 47]. We thus estimate cover semantics via LFAD (frequency-aware Low-Frequency-Aware Decomposition) and suppress them via SFDA (Spatial-Frequency Differential Attention), yielding secret-focused features for FFD. These two modules are integrated with StegaFFD’s server-side facial image analysis network. They can perform frequency-adaptive analysis on stego images in the steganographic domain (separating semantic information and secret information [48]). Specifically, considering that most of the semantic information in the cover belongs to the low-frequency bands, we design LFAD inspired by [49] with low-pass filters to extract the cover image information. To prevent blurring at boundaries, inspired by [50], it predicts spatially variant low-pass filters for the feature instead of using the fixed kernel in the conventional interpolation [49]. Under this operation, LFAD extracts the cover information from concealed facial images, which aids the subsequent SFDA in removing the cover information and extracting the secret information. Next, we propose Spatial-Frequency Differential Attention (SFDA) to enable a global perception of concealed facial images across spatial and spectral dimensions. Through the Differential Transformer, we remove semantic information in the cover images, preventing cover-specific features in the low-frequency band from hindering the extraction of facial related features in the high-frequency bands while ensure global perception.

Moreover, to enhance the practicality of the StegaFFD system and further ensure the accuracy of FFD, motivated by [51], we propose the Steganographic Domain Alignment (SDA) with an auxiliary network to enable the detector to retain more facial and forged features. The training and detection processes are decoupled, meaning that SDA is only employed during training, thereby eliminating the risk of data leakage during detection. During training, SDA extracts clean facial-related features and distills them into the detector network, further enhancing the accuracy of FFD.

Our contributions can be summarized as follows:

- We propose a privacy-enhancing client-server FFD framework, namely StegaFFD, to covertly analyze facial images without raising the suspicions of attackers.
- We design LFAD and SFDA for frequency-aware stego images to ensure that StegaFFD can accurately perform FFD in the steganographic domain without interference from conspicuous information in the covers.
- We develop SDA, which, through the proposed steganographic domain alignment method, further improves the accuracy of the FFD network enhancing the practicality of the StegaFFD.
- Extensive experiments on seven datasets demonstrate the effectiveness and imperceptibility of StegaFFD.

2 Related works

2.1 Facial Privacy Protection

To mitigate privacy risks in face recognition, privacy-preserving face recognition (PPFR) methods operate in protected domains. These methods fall into two categories: (1) Cryptography-Based Methods, which perform recognition on encrypted images using techniques like garbled circuits [52], homomorphic encryption [53], and secure multiparty computation [54]. They maintain accuracy but suffer from high computational costs and lack visualization utility, easily alerting attackers. (2) Transformation-Based Methods, which apply frequency-domain learning [55], generative models [56], and differential privacy [57].

Identifiable Face Anonymization (IDFA) aims to anonymize users' identities while preserving facial characteristics. Existing methods include image obfuscation [58] and face synthesis [59]. Some methods leverage deep models to recognize privacy-protected faces [60]. Li et al. [5, 34] introduced identity-aware anonymization using GANs. Yuan et al. [61] and Zhang et al. [62] proposed steganography-based methods. Wang et al. [63] developed a virtual identity transformation. However, since IDFA modifies images in the original image domain, it transforms non-forged images into forged-like data. As a result, the performance of face forgery detection based on IDFA images is compromised. While PPFR and IDFA focus on recognition under protection

or identity masking, they alter image distribution or reveal processing traces, making them ill-suited for FFD, where fidelity to forgery cues is critical.

2.2 Deep Image Hiding

Image hiding aims to covertly conceal a secret image within a cover image while allowing for accurate extraction of the hidden content. The first deep learning-based image hiding (DIH) networks were introduced by Baluja [64], and Hayes and Danezis [65], utilizing an encoder-decoder architecture. To improve embedding efficiency, [66] incorporated U-Net and discrete wavelet transformation (DWT) [67], enhancing the reversibility of hidden images. The development of invertible neural networks (INNs) in various image-to-image tasks [68, 69] has further advanced image hiding techniques. An INN-based framework is introduced to formulate image embedding and extraction as forward and inverse affine transformations [70]. To achieve higher reversibility and imperceptibility, Deng et al. [43, 44] proposed an INN-based method where both the cover and secret images undergo wavelet transformation. This technique embeds the secret image into the high-frequency components of the cover image, minimizing visible distortions while ensuring accurate recovery.

2.3 Face Forgery Detection

Face forgery detection initially relied on image processing methods (e.g., copy-move, splicing, deletion) to extract inherent features and train machine learning classifiers, such as Speeded-Up Robust Features (SURF) [71] and Photo Response Non-Uniformity (PRNU) [72]. However, these methods often fail against deep learning-generated forgeries (e.g., GAN, VAE). Recent approaches focus on deep networks, including plain deep detector [73–75], spatial deep detector [76, 77], and frequency deep detector [78–80]. 1) Plain detector employs CNNs to directly distinguish face forgery content from authentic data. Numerous CNN-based binary classifiers have been proposed, e.g., MesoNet [73] and Xception [74]. 2) Spatial detector delves deeper into specific representations, such as forgery region location [76], capsule network [77], disentanglement learning [81–83], image reconstruction [84], erasing technology [85], etc. Besides, some other methods specifically focus on the detection of blending artifacts [86], generating forged images during training in a self-supervised manner to boost detector generalization. 3) Frequency detector addresses this limitation by focusing on the frequency domain for forgery detection [80]. SPSL [79] and SRM [87] are other examples of frequency detectors that utilize phase spectrum analysis and high-frequency noises, respectively. Qian et al. [78] propose the use of learnable filters for adaptive mining of frequency forgery clues using frequency-aware image decomposition.

2.4 Privacy Protection in FFD

Previous privacy protection approaches for FFD, such as anonymization, distortion, and encryption, partly mitigate leakage but often introduce

Table 1 Comparison between StegaFFD and other prominent privacy-protection approaches ensuring the security and privacy of facial images during their training, transmission, and analysis processes. The plaintext or encrypted forms of information may raise alerts among malicious actors.

Protection Method	Protection Target	Alert Raising	Acc. Retention
No Protection	—	✓ (Facial Image)	✓
Federated Learning [35, 36]	Training Data	—	✓
Differential Privacy [90]	Training Data	—	✓
Encryption [33]	Testing Data	✓ (Noise)	✓
Distortion [37]	Testing Data	✓ (Distorted Facial Image)	✗
Anonymization [34]	Testing Data	✓ (Facial Image)	✗
StegaFFD (Ours)	Testing Data	✗ (Natural Image)	✓

severe semantic distortion, making images appear obviously protected. Face anonymization methodologies [34] induce synthetic characteristics in genuine images, consequently degrading the detection efficacy of face forgery detection algorithms. Some studies focus on protecting images after deployment through distortion-based [88] methods to modify detailed information of the original images. Although these methods somewhat protect image privacy, attackers can easily notice that the transmitted images are facial images. To further enhance security, some approaches utilize entropy-based methods [89]. However, these methods significantly alter the distribution of the images, easily alerting attackers to the fact that the images are protected by specific techniques, thus falling into a cat-and-mouse game of encryption and decryption. Among these methods, methods based on homomorphic encryption are time-consuming, making them impractical for many real-world applications.

3 Methodology

3.1 Overall Framework

Our StegaFFD consists of an image hiding network $\mathcal{H}(\cdot, \cdot)$, a facial image analysis network $\mathcal{M}(\cdot)$, and a steganographic domain alignment network $\mathcal{M}'(\cdot)$, as illustrated in Fig. 2. The image hiding network $\mathcal{H}(\cdot, \cdot)$ is deployed on the client side, while the facial image analysis network $\mathcal{M}(\cdot)$ runs on the server. The steganographic domain alignment network $\mathcal{M}'(\cdot)$ assists \mathcal{M} in learning facial-relevant features in the steganographic domain and is used only during training. Let \mathbf{x}_{secret} denote the raw facial image captured by user devices (e.g., smartphones or laptops), and let \mathbf{x}_{cover} denote a natural image used as the cover. The hiding process $\mathbf{x}_{stego} = \mathcal{H}(\mathbf{x}_{secret}, \mathbf{x}_{cover})$ produces a stego image in which \mathbf{x}_{secret} is embedded into \mathbf{x}_{cover} . After concealment, \mathbf{x}_{stego} is transmitted from the client to the server and fed directly to the facial image analysis network, yielding the final prediction $\hat{\mathbf{y}} = \mathcal{M}(\mathbf{x}_{stego})$. The facial image analysis network analyzes the concealed facial content in the steganographic domain:

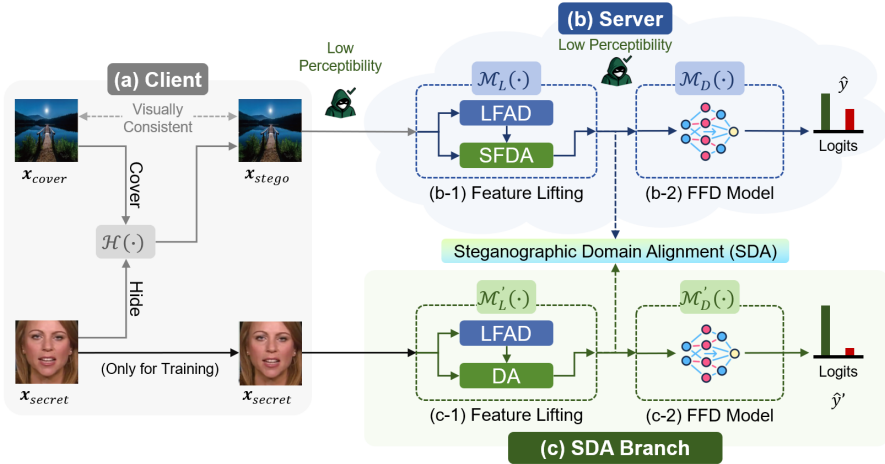


Fig. 2 Illustration of the detailed structure of the proposed StegaFFD. (a) Client-side image hiding network $\mathcal{H}(\cdot)$ hides facial secret images into natural cover images for privacy-preserving transmission. (b) Server-side Detector analyzes stego images directly in the steganographic domain to lift facial features by \mathcal{M}_L for forgery detection. (c) SDA branch enhances detector training by aligning steganographic-domain features with raw facial features lifted by \mathcal{M}'_L , improving forgery detection accuracy. This branch operates exclusively during training and is omitted during deployment.

specifically, \mathcal{M} is divided into a steganographic feature lifting network \mathcal{M}_L and a FFD network \mathcal{M}_D . Meanwhile, during training, the steganographic domain alignment network extracts facial features $f_{secret} = \mathcal{M}'_L(x_{secret})$ to guide \mathcal{M} toward latent facial information. In this pipeline, only x_{stego} can be intercepted by attackers; therefore, x_{stego} must remain visually indistinguishable from x_{cover} to enable covert FFD without arousing suspicion.

3.2 FFD in the Steganographic Domain

We observe that existing FFD methods struggle to perform precise analysis within the steganographic domain. They often produce numerous false alarms (see Table 2, conventional detector), primarily because conspicuous information in the *cover* image interferes with detection. We further notice that most semantic information of the cover is concentrated in the low-frequency band; meanwhile, in image hiding methods, information embedded in higher-frequency components is less likely to be detected than that in lower-frequency components. Therefore, we propose a Low-Frequency-Aware Decomposition (LFAD) to extract the cover semantics and a Spatial-Frequency Differential Attention (SFDA) to suppress its interference from the stego image x_{stego} , thereby enhancing the extraction of x_{secret} .

In our StegaFFD network, the steganographic feature lifting network \mathcal{M}_L consists of LFAD and SFDA. As illustrated in Fig. 3, the stego image x_{stego} is first decomposed into low-frequency features \bar{x} by LFAD. Subsequently, by integrating x_{stego} with \bar{x} , SFDA extracts steganographic-domain features

\mathbf{f}_{stego} that capture the concealed information. Finally, \mathbf{f}_{stego} is processed by the FFD network \mathcal{M}_D to produce the final forgery detection result $\hat{\mathbf{y}}$.

These operations effectively capture secret information, eliminate the influence of the cover image, and improve face forgery detection accuracy within the steganographic domain. In the following sections, we provide detailed descriptions of the proposed LFAD and SFDA.

Low-Frequency-Aware Decomposition

To estimate the cover-level feature, we construct spatially variant low-pass filters to effectively smooth high-frequency components [91]. We propose a Low-Frequency-Aware Decomposition (LFAD) network. Leveraging the advantages of high-level features [92] to achieve high-quality adaptive low-pass filters, the LFAD network takes the hierarchical features \mathbf{x} extracted by the Xception feature network from the stego image \mathbf{x}_{stego} as input and predicts spatial-variant low-pass filters. It comprises a 3×3 convolutional layer followed by a kernel-wise softmax, represented as:

$$\bar{V}^l = \text{Conv}_{3 \times 3}(\mathbf{x}), \bar{W}_{i,j}^{l,p,q} = \text{Softmax}(\bar{V}_{i,j}^l) = \frac{\exp(\bar{V}_{i,j}^{l,p,q})}{\sum_{(p',q') \in \Omega} \exp(\bar{V}_{i,j}^{l,p',q'})}, \quad (1)$$

where $\bar{V}^l \in \mathbb{R}^{\bar{K}^2 \times H \times W}$ stores, at each spatial location (i, j) , \bar{K}^2 logits corresponding to a $\bar{K} \times \bar{K}$ kernel; Ω denotes the index set of offsets within a $\bar{K} \times \bar{K}$ window. The kernel-wise softmax constrains the filter weights to be non-negative and sum to one, yielding smooth low-pass filters $\bar{W} \in \mathbb{R}^{\bar{K}^2 \times H \times W}$ [93]. Consequently, the low-pass filtered features $\bar{\mathbf{x}} \in \mathbb{R}^{C \times H \times W}$ are obtained as:

$$\bar{\mathbf{x}}_{i,j}^l = \sum_{(p,q) \in \Omega} \bar{W}_{i,j}^{l,p,q} \cdot \mathbf{x}_{i+p,j+q}^l, \quad (2)$$

where the operation is applied channel-wise for all C channels (with symmetric padding at boundaries).

Spatial-Frequency Differential Attention

To adaptively remove the cover information from the steganographic image \mathbf{x}_{stego} , we propose Spatial-Frequency Differential Attention (SFDA) as a foundation architecture. Differential attention takes the difference between different softmax attention functions to eliminate cover information and attention noise. Another advantage of this method is its consistency with differential amplifiers [94] proposed in electrical engineering, where the difference between two signals is used as output, so that we can null out the common-mode noise of the input.

We take a decoder-only model as an example to describe the architecture. Given an stego image \mathbf{x}_{stego} and low-pass filtered features $\bar{\mathbf{x}}$, we pack the

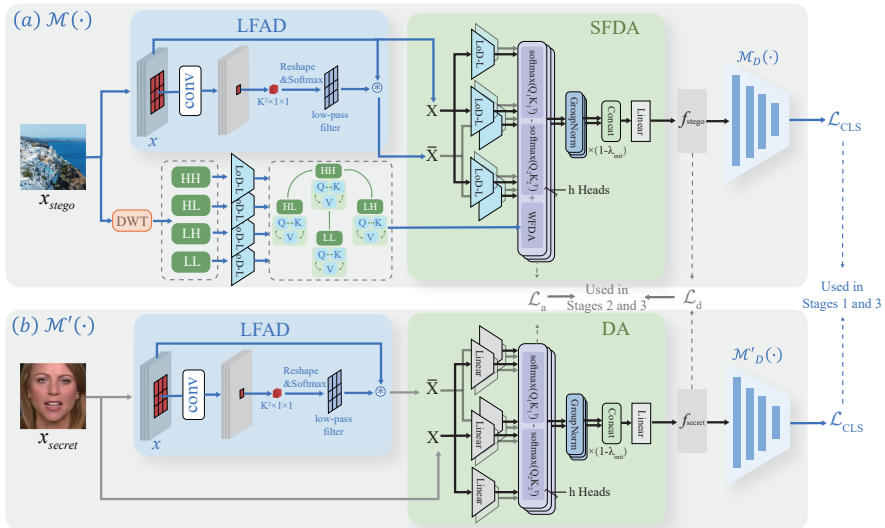


Fig. 3 Illustration of (a) the server-side network $\mathcal{M}(\cdot)$ of the proposed LFAD and SFDA. The feature lifting network contains LFAD and SFDA, which extracts high-frequency steganographic features containing facial information. (b) SDA branch $\mathcal{M}'(\cdot)$ helps to lift secret facial features by aligning stego-domain features with raw facial features.

input embeddings into $\mathbf{X} \in \mathbb{R}^{(H \times W) \times C}$ and $\bar{\mathbf{X}} \in \mathbb{R}^{(H \times W) \times C}$. The input is further contextualized to obtain the output \mathbf{f}_{stego} , i.e., $\mathbf{f}_{stego} = \text{Decoder}(\mathbf{X}, \bar{\mathbf{X}})$. The decoder consists of two modules: a differential attention module followed by a feed-forward network module. Compared to vanilla Transformer [95–97], the main difference is the replacement of conventional softmax attention with differential attention, while the macro layout is kept the same. We also adopt pre-RMSNorm [98] as improvements following LLaMA [99].

The differential attention mechanism maps query, key, and value vectors to outputs. We use query and key vectors to compute attention scores, and then compute a weighted sum of value vectors. The critical design is that we use a pair of softmax functions to extract secret information and cancel the noise of attention scores.

Given input features \mathbf{X} and $\bar{\mathbf{x}}$ (flattened to the same shape as \mathbf{X}), we project them into query, key, and value representations using linear transformations:

$$Q_1 = \mathbf{X}W^Q, Q_2 = \bar{\mathbf{x}}W^{LQ}, K_1 = \mathbf{X}W^K, K_2 = \bar{\mathbf{x}}W^{LK}, V = \mathbf{X}W^V, \quad (3)$$

where $Q_1, Q_2, K_1, K_2, V \in \mathbb{R}^{(H \times W) \times d}$, and all W are learnable projection matrices. We apply pre-normalization (RMSNorm) to token embeddings before projections to stabilize training.

To capture more comprehensive frequency information, we further decompose \mathbf{X} using the discrete wavelet transform (DWT) into four sub-bands:

$$\mathbf{x}^{LL}, \mathbf{x}^{LH}, \mathbf{x}^{HL}, \mathbf{x}^{HH} = \text{DWT}(\mathbf{X}), \quad \mathbf{x}^{(\cdot)} \in \mathbb{R}^{\left(\frac{H}{2} \times \frac{W}{2}\right) \times C}. \quad (4)$$

Each sub-band is projected separately into queries and keys:

$$\begin{aligned} Q_{hh} &= \mathbf{x}^{HH} W^{hhQ}, & Q_{hl} &= \mathbf{x}^{HL} W^{hlQ}, & Q_{lh} &= \mathbf{x}^{LH} W^{lhQ}, & Q_{ll} &= \mathbf{x}^{LL} W^{llQ}, \\ K_{hh} &= \mathbf{x}^{HH} W^{hhK}, & K_{hl} &= \mathbf{x}^{HL} W^{hlK}, & K_{lh} &= \mathbf{x}^{LH} W^{lhK}, & K_{ll} &= \mathbf{x}^{LL} W^{llK}. \end{aligned} \quad (5)$$

The wavelet frequency-differential attention is computed as:

$$\begin{aligned} \text{WFDA}(\mathbf{X}) &= \text{softmax}\left(\frac{Q_{hh}K_{hh}^\top}{\sqrt{d}}\right) + \text{softmax}\left(\frac{Q_{hl}K_{hl}^\top}{\sqrt{d}}\right) \\ &\quad - \text{softmax}\left(\frac{Q_{lh}K_{lh}^\top}{\sqrt{d}}\right) - \text{softmax}\left(\frac{Q_{ll}K_{ll}^\top}{\sqrt{d}}\right). \end{aligned} \quad (6)$$

The final differential attention operator is defined as:

$$\text{DiffAttn}(\mathbf{X}, \bar{\mathbf{x}}) = \text{softmax}\left(\frac{Q_1K_1^\top}{\sqrt{d}}\right) - \lambda \text{softmax}\left(\frac{Q_2K_2^\top}{\sqrt{d}}\right) + \text{WFDA}(\mathbf{X}), \quad (7)$$

Here, $W^Q, W^{LQ}, W^K, W^{LK}, W^V \in \mathbb{R}^{C \times d}$ are learnable projection matrices, and λ is a learnable scalar. To facilitate stable optimization, we re-parameterize λ as:

$$\lambda = \exp(\lambda_{q_1} \cdot \lambda_{k_1}) - \exp(\lambda_{q_2} \cdot \lambda_{k_2}) + \lambda_{\text{init}}, \quad (8)$$

where $\lambda_{q_1}, \lambda_{k_1}, \lambda_{q_2}, \lambda_{k_2} \in \mathbb{R}^d$ are learnable vectors, and $\lambda_{\text{init}} \in (0, 1)$ is a constant initialization value. In practice we also clamp λ into $[0, 1]$ to prevent numerical explosion; setting $\lambda_{\text{init}} = 0.8$ works well empirically.

To mitigate the loss of effective resolution caused by averaging attention weights across spatial positions, we further adopt the multi-head attention mechanism [95] in our Differential Attention module. Let h denote the number of attention heads. For each head $i \in [1, h]$, we use separate projection matrices $W_i^Q, W_i^{LQ}, W_i^K, W_i^{LK}, W_i^V$, while sharing the same scalar λ across all heads within a layer. The output of each head is normalized and aggregated as follows:

$$\begin{aligned} \text{head}_i &= \text{DiffAttn}(\mathbf{X}, \bar{\mathbf{x}}; W_i^Q, W_i^{LQ}, W_i^K, W_i^{LK}, \lambda) V_i, \\ \overline{\text{head}_i} &= (1 - \lambda_{\text{init}}) \cdot \text{LN}(\text{head}_i), \\ \text{MultiHead}(\mathbf{X}, \bar{\mathbf{x}}) &= \text{Concat}(\overline{\text{head}_1}, \dots, \overline{\text{head}_h}) W^O, \end{aligned} \quad (9)$$

where $V_i = \mathbf{X}W_i^V \in \mathbb{R}^{(H \times W) \times d}$, $\text{LN}(\cdot)$ applies RMSNorm [98] to each head independently, and $\text{Concat}(\cdot)$ denotes concatenation along the channel dimension.

We apply a fixed scaling factor $(1 - \lambda_{\text{init}})$ to RMSNorm outputs to maintain gradient alignment with standard Transformer architectures. We set the number of heads as $h = \frac{H \times W}{2d}$, where d is the per-head feature dimension consistent with standard Transformer settings. The output projection matrix is $W^O \in \mathbb{R}^{(h \cdot d) \times C}$.

As illustrated in Fig. 3, we use GroupNorm(\cdot) [100] emphasize that LN(\cdot) is applied to each head independently. As differential attention tends to have a sparser pattern, statistical information is more diverse between heads. The LN(\cdot) operator normalizes each head before concatenation to improve gradient statistics [101–103].

Finally, we describe the architecture of the Multi-Head Differential Attention network as:

$$\mathbf{f}_{\text{stego}} = \lambda_d \cdot \text{MultiHead}(\text{LN}(\mathbf{X}, \bar{\mathbf{X}})) + \mathbf{X}, \quad (10)$$

where LN(\cdot) is RMSNorm [98], λ_d is hyperparameter. Here LN($\mathbf{X}, \bar{\mathbf{X}}$) denotes applying normalization after concatenating \mathbf{X} and $\bar{\mathbf{X}}$ along channels.

3.3 Steganographic Domain Alignment

To guide the $\mathcal{M}_L(\mathbf{x}_{\text{stego}})$ network to retain more information about $\mathbf{x}_{\text{secret}}$, we design an alignment method. Steganographic Domain Alignment (SDA) network extracts the steganographic-domain features of the secret image, denoted as $\mathbf{f}_{\text{secret}}$, and guides $\mathcal{M}_L(\mathbf{x}_{\text{stego}})$ to align with $\mathbf{f}_{\text{secret}}$ when extracting the steganographic-domain features of the stego image. Notably, the SDA network is only involved during the training phase.

$$\mathbf{f}_{\text{secret}} = \mathcal{M}'_L(\mathbf{x}_{\text{secret}}). \quad (11)$$

\mathcal{M}'_L network is also a decoder-only model. Its attention matrix is denoted as

$$\begin{aligned} \bar{\mathbf{x}}_{\text{secret}} &= \text{LFAD}(\mathbf{x}_{\text{secret}}), \\ \text{DiffAttn}(\mathbf{x}_{\text{secret}}, \bar{\mathbf{x}}_{\text{secret}}) &= \text{softmax}\left(\frac{Q_1 K_1^\top}{\sqrt{d}}\right) - \lambda \cdot \text{softmax}\left(\frac{Q_2 K_2^\top}{\sqrt{d}}\right), \end{aligned} \quad (12)$$

where $X = \mathbf{x}_{\text{secret}}$, $\bar{\mathbf{x}} = \bar{\mathbf{x}}_{\text{secret}}$, and Q_1, Q_2, K_1, K_2 are computed as in Eq. (3) (row-wise softmax). We use the same λ re-parameterization as Eq. (8). We note this attention network as Differential Attention (DA).

Steganographic Domain Distance Metric

To align features in the steganographic domain, we must choose an appropriate distance between the stego and secret features. In domain adaptation, two families of metrics are commonly used: (i) moment-estimation criteria, such as MMD [104], CORAL [105], and HoMM [106]; and (ii) information-theoretic divergences comparing distributions, including KL [107], JS [108], and Wasserstein [109].

Considering both training stability and the subtle distribution shift introduced by information embedding, we adopt CORAL as the core of SDA, as it is effective at capturing slight discrepancies [110]. At the same time, because MMD primarily reflects the mean shift between domains, we use it as a dynamic coefficient to modulate the overall alignment strength. Concretely, our SDA distance is

$$d_{SDA}(\mathbf{f}_{stego}, \mathbf{f}_{secret}) = d_C(\mathbf{f}_{stego}, \mathbf{f}_{secret}) \cdot \exp(\gamma d_M(\mathbf{f}_{stego}, \mathbf{f}_{secret})), \quad (13)$$

where d_C and d_M denote the standard CORAL and MMD distances, respectively; γ is a fixed hyperparameter (we set $\gamma = 10$). Here, \mathbf{f}_{secret} is the feature lifted from the feature lifting network.

The loss function for aligning the steganographic domain is designed as

$$\mathcal{L}_d = d_{SDA}(\mathbf{f}_{stego}, \mathbf{f}_{secret}). \quad (14)$$

Low-rank Decomposition fine-tuning

Our experiments reveal that directly applying the \mathcal{L}_{SDA} loss can sometimes degrade the recognition accuracy of the FFD network, suggesting that the alignment branch interferes with already learned representations. To minimize disruption to the well-learned semantic knowledge, inspired by [111], we incorporate Low-rank Decomposition (LoD) to explicitly separate an orthogonal *semantic* subspace from a *forgery-specific* subspace, thereby preventing distortion of acquired semantics during steganographic domain alignment.

We obtain a rank- r approximation of the pre-trained weight matrix with LoD in stage 1 (3.4); that is, we retain only the top r singular values and the associated singular vectors:

$$W_r = U_r \Sigma_r V_r^\top, \quad (15)$$

where $U_r \in \mathbb{R}^{n \times r}$, $\Sigma_r \in \mathbb{R}^{r \times r}$, and $V_r \in \mathbb{R}^{n \times r}$. We keep W_r frozen throughout subsequent training stages to preserve knowledge learned from stage 1 training.

The residual component is defined as the difference between the full weights and the LoD approximation:

$$\Delta W = W - W_r = U_{n-r} \Sigma_{n-r} V_{n-r}^\top, \quad (16)$$

where $U_{n-r} \in \mathbb{R}^{n \times (n-r)}$, $\Sigma_{n-r} \in \mathbb{R}^{(n-r) \times (n-r)}$, and $V_{n-r} \in \mathbb{R}^{n \times (n-r)}$. Note that ΔW is the learnable part, corresponding to the remaining singular components and reflecting slight, targeted adjustments to the original weight matrix.

During training, we optimize only ΔW while keeping U_r , Σ_r , and V_r fixed. This implementation preserves stage 1 semantics via W_r and adapts the model to align the steganographic domain through the residual ΔW . We evaluate $n - r \in \{1, 4, 16, 64\}$ and observe that $n - r = 16$ yields the best performance.

Algorithm 1 Training Process of StegaFFD

Require: DIH network \mathcal{H} , SDA networks $(\mathcal{M}'_L, \mathcal{M}'_D)$, StegaFFD feature lifting network \mathcal{M}_L , FFD network \mathcal{M}_D , training set \mathcal{T} , stage epochs (e_1, e_2, e_3) , learning rates $(\ell_r^1, \ell_r^2, \ell_r^3)$

- 1: $E \leftarrow e_1 + e_2 + e_3$
- 2: **for** $j = 1$ to E **do**
- 3: **for** each $(\mathbf{x}_{cover}, \mathbf{x}_{secret}, \mathbf{y}) \in \mathcal{T}$ **do**
- 4: $\mathbf{x}_{stego} \leftarrow \mathcal{H}(\mathbf{x}_{cover}, \mathbf{x}_{secret})$
- 5: $\bar{\mathbf{x}} \leftarrow \text{LFAD}(\mathbf{x}_{stego})$
- 6: $\bar{X}, X \leftarrow \bar{\mathbf{x}}, \mathbf{x}_{stego}$
- 7: $\mathbf{f}_{stego} \leftarrow \text{SFDA}(\bar{X}, X)$
- 8: $\mathbf{f}_{secret} \leftarrow \mathcal{M}'_L(\mathbf{x}_{secret})$
- 9: **if** $j \leq e_1$ **then** \triangleright Stage 1: train $\mathcal{M}, \mathcal{M}'$ with \mathcal{L}_{CLS} ; freeze \mathcal{H}
- 10: $\hat{\mathbf{y}} \leftarrow \mathcal{M}_D(\mathbf{f}_{stego}), \hat{\mathbf{y}}' \leftarrow \mathcal{M}'_D(\mathbf{f}_{stego})$
- 11: $\mathcal{L}_{CLS} \leftarrow \text{Eq. (19)}$
- 12: $\theta_{\mathcal{M}, \mathcal{M}'} \leftarrow \theta_{\mathcal{M}, \mathcal{M}'} - \ell_r^1 \cdot \nabla_{\theta_{\mathcal{M}, \mathcal{M}'}} \mathcal{L}_{CLS}$
- 13: **else if** $e_1 < j \leq e_1 + e_2$ **then** \triangleright Stage 2: align \mathcal{M}_L with \mathbf{f}_{secret} ; freeze \mathcal{H}
- 14: $\mathcal{L}_d \leftarrow \text{Eq. (13)}, \mathcal{L}_a \leftarrow \text{Eq. (17)}$
- 15: $\mathcal{L}_{SDA} \leftarrow \mathcal{L}_d + \mathcal{L}_a$
- 16: $\theta_{\mathcal{M}_L} \leftarrow \theta_{\mathcal{M}_L} - \ell_r^2 \cdot \nabla_{\theta_{\mathcal{M}_L}} \mathcal{L}_{SDA}$
- 17: **else** \triangleright Stage 3: joint fine-tuning of \mathcal{M} and \mathcal{H} with \mathcal{L}_{total}
- 18: $\hat{\mathbf{y}} \leftarrow \mathcal{M}_D(\mathbf{f}_{stego}), \hat{\mathbf{y}}' \leftarrow \mathcal{M}'_D(\mathbf{f}_{secret})$
- 19: $\mathcal{L}_{CLS} \leftarrow \text{Eq. (19)}, \mu \leftarrow \text{Eq. (21)}$
- 20: $\mathcal{L}_{total} \leftarrow \mathcal{L}_{CLS} + \mu \mathcal{L}_{SDA}$ \triangleright See Eq. (20)
- 21: $\theta_{\mathcal{M}} \leftarrow \theta_{\mathcal{M}} - \ell_r^3 \cdot \nabla_{\theta_{\mathcal{M}}} \mathcal{L}_{total}$
- 22: $\theta_{\mathcal{H}} \leftarrow \theta_{\mathcal{H}} - \ell_r^3 \cdot \nabla_{\theta_{\mathcal{H}}} \mathcal{L}_{total}$
- 23: **end if**
- 24: **end for**
- 25: **end for**

Attention Alignment

To align the domain-invariant features extracted by the StegaFFD feature lifting network, we update the network by minimizing the distribution distance between the stego and secret features. In addition, to further couple the information captured by the feature lifting network and SDA branches, we introduce an attention-alignment term. For each stego–secret pair, the loss is

$$\mathcal{L}_a = \|\mathbf{A}_{stego} - \mathbf{A}_{secret}\|_F^2, \quad (17)$$

where $\mathbf{A}_{stego} = \text{DiffAttn}(X, \bar{X})$, and $\mathbf{A}_{secret} = \text{DiffAttn}(\mathbf{x}_{secret}, \bar{\mathbf{x}}_{secret})$.

Finally, we present the whole loss function for the alignment of the steganographic domain

$$\mathcal{L}_{SDA} = \mathcal{L}_d + \mathcal{L}_a. \quad (18)$$

3.4 Training Process

We use a multi-stage training strategy for StegaFFD, as shown in Algorithm 1. **Stage 1:** We freeze the pretrained DIH network and train the facial image analysis network (together with the SDA branch) using the classification loss \mathcal{L}_{CLS} . **Stage 2:** We continue freezing the DIH network and *align* lifted features with \mathbf{f}_{secret} by minimizing \mathcal{L}_{SDA} . **Stage 3:** We fine-tune the whole StegaFFD (i.e., the DIH and facial image analysis networks) under the total loss \mathcal{L}_{total} .

$$\mathcal{L}_{CLS} = -\frac{1}{N_b} \sum_{i=1}^{N_b} \left[\mathbf{y}_i \log(\hat{\mathbf{y}}_i) + (1 - \mathbf{y}_i) \log(1 - \hat{\mathbf{y}}_i) + \mathbf{y}_i \log(\hat{\mathbf{y}}'_i) + (1 - \mathbf{y}_i) \log(1 - \hat{\mathbf{y}}'_i) \right]. \quad (19)$$

The total loss in model training is then defined as:

$$\mathcal{L}_{total} = \mathcal{L}_{CLS} + \mu \cdot \mathcal{L}_{SDA}, \quad (20)$$

where μ is a hyperparameter that balances the two losses. During training, μ is gradually increased with the number of iterations so that the cross-entropy term dominates early training and helps learn discriminative stego features:

$$\mu = \frac{2}{1 + \exp(-\gamma_s \cdot \frac{s_t}{s_T})} - 1, \quad (21)$$

where s_t denotes the current training step, s_T represents the total number of training steps and γ_s is a hyperparameter, set to $\gamma_s = 10$ in our experiments. The range of μ gradually increases from 0 to 1 over the course of training.

4 Experiment

4.1 Experimental Setup

Datasets. For comprehensive comparisons, we use a collection of eight widely recognized and extensively used datasets in the realm of face forgery detection: FaceForensics++ [74], CelebDF-v1 [112], CelebDF-v2 [112], DeepFakeDetection [113], DeepFake Detection Challenge Preview [114], DeepFake Detection Challenge [115], UADFV [116] and FaceShifter [117]. FaceForensics++ consists of 1,000 real and 4,000 fake videos generated by four distinct deepfake synthesis methods. CelebDF-v1 (CDFv1) contains 408 real and 795 fake videos primarily created using one high-quality deepfake method. CelebDF-v2 (CDFv2) is an upgraded version of v1, it features 590 real and 5,639 fake videos forged with an improved version of a single method. DeepFakeDetection (DFD) includes 363 real and 3,000 fake videos generated from five different synthesis techniques. DeepFake Detection Challenge Preview (DFDCP) contains 1,131 real and 4,119 fake videos from two methods, it also incorporates three types of perturbations. DeepFake Detection Challenge (DFDC) is a massive dataset

with 23,654 real and 104,500 fake videos produced by eight methods and includes 19 perturbations. UADFV is a smaller-scale dataset, it consists of 49 real and 49 fake videos created using one deepfake method. FaceShifter (Fsh) contains 1,000 real and 1,000 fake videos forged using a single, high-fidelity face-swapping technique. FaceForensics++ is employed for model training, while the rest are frequently used as testing data.

Competing Detectors. To the best of our knowledge, no method has been proposed to perform FFD in the steganographic domain. To ensure a comprehensive and fair comparison, we select a **face anonymization method** Falco [118] and four widely used **DIH methods** (i.e., WengNet [119], HiD-DeN [120], BalujaNet [121] and HiNet [122]) to perform privacy-preserving. Then we deploy four famous or SOTA face forgery detection networks, i.e., Xception [74], Meso4 [73], MesoIncep [73], and F3Net [78]. We pair each privacy-preserving method with each FFD network, forming twenty competing methods.

Evaluation Metrics. Regarding evaluation, we compute the average value of the top-3 metrics, such as the average top-3 area under the curve (AUC). Additionally, we report the top-1 results. Other widely used metrics, including accuracy (ACC), average precision (AP), and equal error rate (EER), are also computed and presented in the following sections.

Implementation Details. In the data processing, face detection, face cropping, and alignment are performed using DLIB [123]. The aligned faces are resized to 256×256 for both the training and testing. We also apply widely used data augmentations, i.e., image compression, horizontal flip, rotation, Gaussian blur, and random brightness contrast. In the training module, we use the Adam optimizer with learning rates $\ell_r^1, \ell_r^2, \ell_r^3$ of $2 \times 10^{-4}, 1 \times 10^{-4}, 1 \times 10^{-5}$, respectively. The batch size is fixed at 32 for all experiments. We set $\lambda_{init}, \lambda_d$ of SFDA shown in Eq. (8,10) to 0.8, 2. We primarily leverage pre-trained backbones from ImageNet if feasible. Otherwise, we resort to initializing the remaining weights using a normal distribution. During training, all cover images \mathbf{x}_{cover} are randomly selected.

4.2 Comparison Results

Classification Results. As shown in Table 2, StegaFFD achieves the highest detection performance across seven datasets compared to other covert FFD methods, respectively. On average, its segmentation performance surpasses that of the second-place Xception + HiNet by 5.16% in AUC. When compared to the vanilla framework (without privacy-enhancing) utilizing Xception, StegaFFD’s average performance only shows a slight decrease of 1.96% in AUC. This indicates StegaFFD’s effectiveness in maintaining high FFD performance while enhancing privacy protection. We note that F3Net also utilizes information from the frequency domain and extracts frequency artifacts for detection (similar to StegaFFD), but underperforms due to its lack of adaptive analysis

Table 2 Cross-domain evaluations using the AUC (%) metric. All detectors are trained on FF-c23 and evaluated on other data. “Avg.” denotes the average AUC for within-domain and cross-domain evaluation, and the overall results. “Top-3” represents the count of each method’s ranks within the top-3 across all testing datasets. “Freq.” denotes the frequency type. Privacy Preserving method include (i) unprotected (None), (ii) an anonymization method (Falco [118]), (iii) existing steganography method (HiNet [122] to BalujaNet [121]). The best-performing method for each column is highlighted in **red** and the top three are shown in **bold**.

Privacy Preserving	Type	FFD Detector	Cross Domain Evaluation								
			CDFv1	CDFv2	DFD	DFDC	DFDCP	Fsh	UADFV	Avg.	Top-3
None	Plain	Xception	74.85	75.97	82.11	69.19	68.11	59.48	88.01	73.96	—
None	Plain	Meso4	63.69	55.65	52.97	58.89	49.03	52.90	59.05	56.03	—
None	Plain	MesoIncep	70.84	70.02	59.80	60.16	74.57	69.21	89.78	70.63	—
None	Freq.	F3Net	62.91	64.89	83.88	66.61	70.84	72.66	77.76	71.36	—
Falco	Plain	Xception	69.12	65.41	59.49	58.54	61.92	54.98	51.48	60.13	0
Falco	Plain	Meso4	45.35	55.93	49.23	50.82	55.81	54.06	53.10	52.04	0
Falco	Plain	MesoIncep	58.34	62.56	50.15	50.77	61.40	54.43	60.48	56.88	0
Falco	Freq.	F3Net	56.53	59.04	56.59	52.91	62.32	54.54	50.01	55.99	0
HiNet	Plain	Xception	74.94	66.94	70.40	63.85	64.26	47.01	80.49	66.84	0
HiNet	Plain	Meso4	64.11	60.60	50.61	52.09	55.29	50.38	53.01	55.16	0
HiNet	Plain	MesoIncep	57.78	62.56	58.77	57.86	71.73	62.15	78.21	64.15	3
HiNet	Freq.	F3Net	72.45	71.08	71.83	63.40	60.59	53.13	68.04	65.79	1
HiDDeN	Plain	Xception	68.96	64.27	72.07	63.80	64.45	49.64	74.36	65.51	2
HiDDeN	Plain	Meso4	63.93	64.65	53.32	56.13	57.90	56.94	76.31	61.31	0
HiDDeN	Plain	MesoIncep	65.64	67.99	58.34	60.47	69.25	61.72	73.56	65.28	2
HiDDeN	Freq.	F3Net	68.80	69.55	69.02	63.13	62.42	57.15	68.24	65.47	0
WengNet	Plain	Xception	67.70	66.23	70.5	64.01	65.74	50.44	75.81	65.78	0
WengNet	Plain	Meso4	51.66	58.16	51.89	52.23	59.16	53.64	60.80	55.36	0
WengNet	Plain	MesoIncep	60.07	57.47	52.48	50.74	52.98	50.23	52.14	53.73	0
WengNet	Freq.	F3Net	76.40	72.17	70.38	60.86	62.52	53.35	69.78	66.49	2
BaluaNet	Plain	Xception	70.56	68.90	75.55	62.61	63.15	50.75	74.05	65.22	1
BaluaNet	Plain	Meso4	62.48	62.40	50.70	52.68	58.86	50.85	66.14	57.73	0
BaluaNet	Plain	MesoIncep	66.24	64.05	61.52	61.41	66.96	63.50	75.47	65.59	1
BaluaNet	Freq.	F3Net	60.48	65.93	76.36	61.82	66.88	58.52	65.32	65.04	0
HiDDeN	Freq.	SFDA	72.57	66.20	80.23	55.20	68.85	53.04	66.05	66.02	1
HiDDeN	Freq.	SFDA+SDA	77.15	72.41	81.47	52.09	65.78	50.03	50.04	64.14	3
HiDDeN	Freq.	StegaFFD	81.22	72.43	80.64	66.40	71.03	58.68	73.63	72.00	5

across different frequencies of the stego image. Additionally, despite Meso4, MesoIncep, and F3Net having incremental designs over Xception, their performance does not improve across all datasets. This inconsistency can be attributed to the fact that their incremental designs are not effective in the steganographic domain.

Secret Sensibility. As shown in Fig. 4, \mathbf{x}_{stego} generated by DIH has the highest visual similarity to \mathbf{x}_{cover} , thereby enhancing facial privacy protection. To demonstrate that the features extracted by StegaFFD are cover-agnostic, we conduct an attribution analysis on the feature space (\mathbf{f}_{stego}). Utilizing the GradCAM [124] algorithm, it is evident that StegaFFD’s feature space (\mathbf{f}_{stego}) is primarily focused on facial forgery regions (e.g., eyes, nose, and mouth)

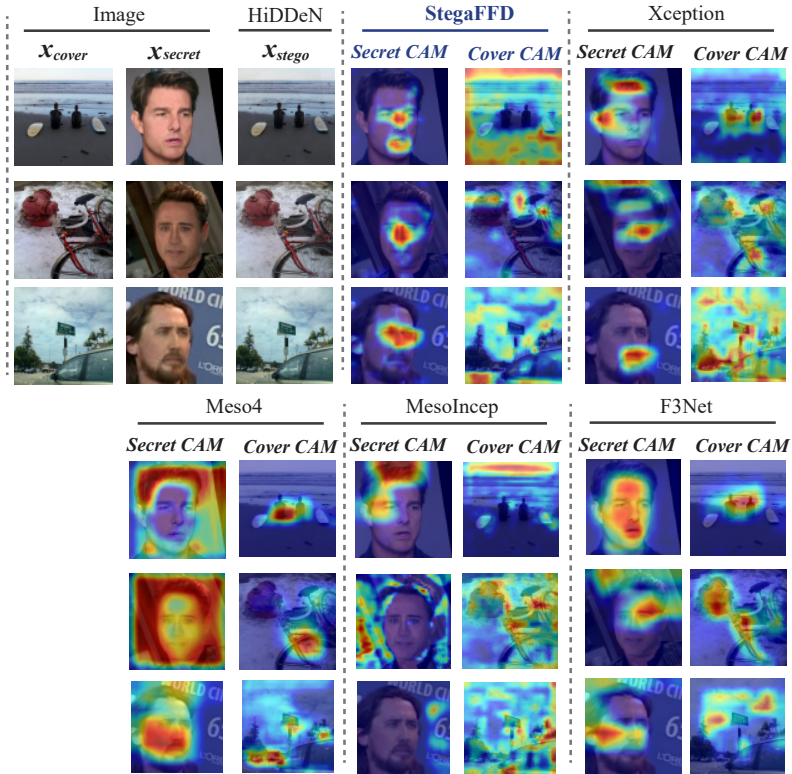


Fig. 4 Visual attribution analysis of face forgery detection algorithms (i.e., StegaFFD, Xception [74], Meso4 [73], MesoIncep [73], and F3Net [78]) using Grad-CAM++, highlighting feature focus on cover and secret image regions (e.g., facial forgery areas).

while remaining insensitive to the main content of the cover image. In contrast, other algorithms either suffer from significant influence by the cover’s semantic information (e.g., Meso4, F3Net) or fail to extract effective semantic features (e.g., MesoIncep). The poor secret sensibility of competing methods is attributed to the absence of low-frequency guidance from \mathbf{x}_{stego} . To demonstrate the robustness of our algorithm across different natural cover images, we embed a single face image into four distinct natural cover images, as shown in Fig. 5, with attribution results indicating that StegaFFD consistently focuses on the face region, exhibiting strong robustness.

We quantify the results of an attribution analysis to determine whether the detectors prioritize the embedded face content over the natural cover image in our steganographic setting (Fig. 6). For StegaFFD and four baseline detectors, we generate per-image heatmaps from intermediate feature activations. We then calculate an attention score using a JET-colormap-aware, color-weighted metric, where higher red intensity and lower blue intensity reflect stronger attention. We analyze twenty pairs of face images and cover images. The data

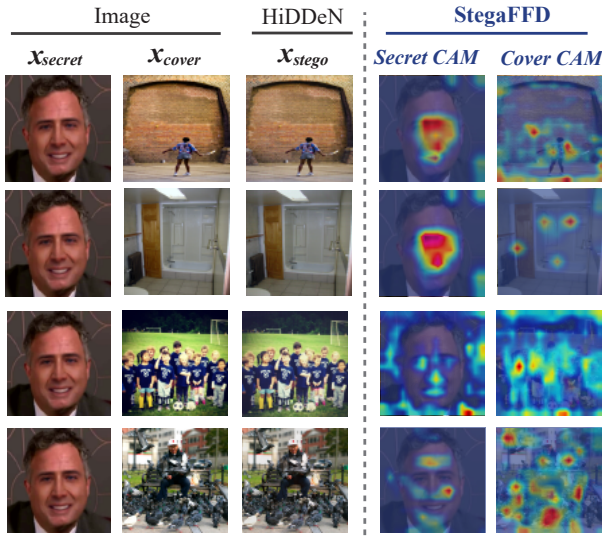


Fig. 5 Robust attribution analysis of face forgery detection across varied cover images for a single facial instance and failure cases. This figure illustrates Grad-CAM++ attribution heatmaps highlighting feature focus on cover and secret image regions (e.g., facial forgery areas).

Table 3 Similarity metrics PSNR and SSIM for image pairs $\mathbf{x}_{cover}/\mathbf{x}_{stego}$ and $\mathbf{x}_{secret}/\mathbf{x}_{stego}$, demonstrating StegaFFD’s imperceptibility.

Image Pair	PSNR \uparrow	SSIM \uparrow
$\mathbf{x}_{cover}/\mathbf{x}_{stego}$	32.46	0.86
$\mathbf{x}_{secret}/\mathbf{x}_{stego}$	10.38	0.41

is categorized into “face” and “cover” sets for each algorithm and evaluated using the mean attention score as the primary metric, with quartile lines for additional robustness checks. Violin plots visualize the attention score distributions across algorithms. We apply two-sample t-tests to assess differences between face and cover attention groups. Results show that StegaFFD exhibits a significantly larger separation between face and cover attention distributions compared to the baseline detectors. Its face attention scores are consistently higher, with stronger statistical significance, demonstrating that StegaFFD more effectively focuses on the embedded face content rather than the cover image.

Imperceptibility As shown in Fig. 4 and Fig. 5, \mathbf{x}_{stego} generated by DIH has the highest visual similarity to \mathbf{x}_{cover} , thereby enhancing facial privacy protection. We also analyzed the similarity between \mathbf{x}_{cover} and \mathbf{x}_{stego} , as well as between \mathbf{x}_{secret} and \mathbf{x}_{stego} . We reported PSNR and SSIM to quantify their similarity. The results indicate that \mathbf{x}_{cover} and \mathbf{x}_{stego} are highly similar, demonstrating that StegaFFD has excellent imperceptibility (Table 3).

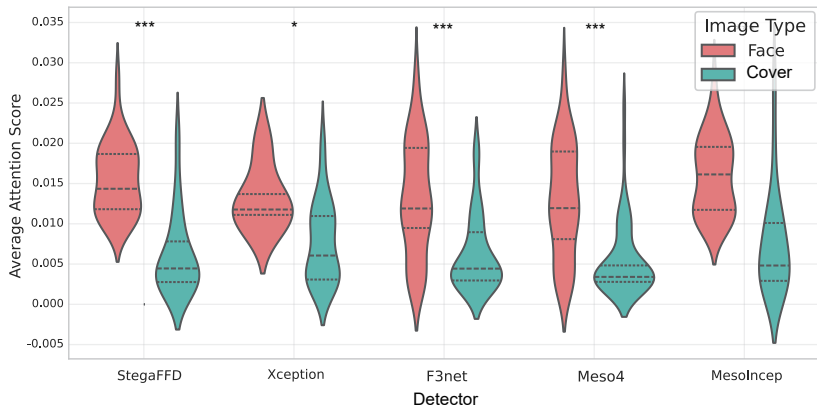


Fig. 6 Quantitative attribution analysis using violin plots comparing attention to embedded face regions versus natural backgrounds across detectors. StegaFFD exhibits a markedly larger face–natural separation than the four baselines, indicating stronger, more consistent focus on face content.



Fig. 7 Comparison of imperceptibility between StegaFFD and anonymization-based methods. StegaFFD hides facial information within natural images, achieving higher imperceptibility, while anonymization-based methods introduce face forgery features, leading to reduced FFD accuracy.

To further compare the advantages of StegaFFD and anonymization-based methods in terms of imperceptibility, we conducted a separate comparison in Fig. 7. Although anonymization-based methods modify facial identity information, they introduce face forgery features, resulting in a disadvantage in FFD accuracy. In contrast, StegaFFD hides facial information within natural images, making privacy information less perceptible.

Failure Cases To better inform the community about the advantages and limitations of StegaFFD, and to avoid failures in practical applications, we analyzed the failure cases of StegaFFD. The last two rows of Fig. 5 showcase

Table 4 Ablation results for SFDA variants on CDFv1 and CDFv2 datasets. All metrics in the table are presented as percentages.

Variation of SFDA	CDFv1				CDFv2			
	AUC ↑	ACC↑	AP↑	EER ↓	AUC ↑	ACC↑	AP↑	EER ↓
LFAD	53.04	38.36	54.05	47.38	58.18	34.22	61.72	44.43
HFAD	64.15	65.33	62.84	39.48	60.44	64.78	65.64	40.10
w/o DWT	73.20	62.24	81.57	32.00	71.46	66.12	73.51	33.77
StegaFFD	81.22	71.25	86.93	24.85	72.43	70.68	82.95	26.62

Table 5 Ablation study on SDA Loss formulations for StegaFFD on CDFv1 datasets. All metrics in the table are presented as percentages.

SDA Loss	AUC ↑	ACC↑	AP↑	EER ↓
None	72.57	62.21	79.04	31.92
FA(12) loss	73.20	63.99	75.46	34.33
AA(sda) loss	70.88	66.35	78.49	36.24
FA(12)+AA(12) loss	75.31	63.23	81.96	30.25
FA(sda)+AA(sda) loss	79.65	65.63	84.35	27.09
FA(12)+AA(sda) loss	81.22	71.25	86.93	24.85

these failure cases. When the cover image contains densely packed objects, it may affect detection results. This is because our method focuses on extracting high-frequency information from steganographic images. If the cover image itself contains dense objects, it generates high-frequency information, which may interfere with the detector. Therefore, in practical use, selecting natural images with less dense objects as covers can help avoid potential issues.

4.3 Ablation Study

Effectiveness of SFDA. To validate the effectiveness of SFDA in extracting secret information, we deploy several variants of SFDA. 1) We directly apply low-frequency filters to extract the low-frequency signal \bar{x} as the feature f_{stego} , denoted as Direct LFAD. 2) We reformulated the filters $\bar{W}_{i,j}^{l,p,q}$ in Eq. 1 as high-pass filters,

$$\bar{W}_{i,j}^{p,q} = \mathbb{E}^{p,q} - \text{Softmax}(\bar{V}_{i,j}^{l,p,q}) = \mathbb{E}^{p,q} - \frac{\exp(\bar{V}_{i,j}^{l,p,q})}{\sum_{(p',q') \in \Omega} \exp(\bar{V}_{i,j}^{l,p',q'})}. \quad (22)$$

To ensure the final generated kernels \bar{W} are high-pass, we follow [83] to invert the low-pass kernels by subtracting them from the identity kernel \mathbb{E} , whose weights are $[[0, 0, 0], [0, 1, 0], [0, 0, 0]]$ when $\bar{K} = 3$. Ω denotes the index set of offsets within a $\bar{K} \times \bar{K}$ window. We note it as HFAD. 3) We remove the discrete wavelet transformation (DWT) from the differential attention mechanism, referred to as w/o DWT.

Table 6 Comparison of detection performance with and without LoD across CDFv1, CDFv2, and UADFV datasets. All metrics in the table are presented as percentages.

LoD	CDFv1		CDFv2		UADFV	
	w/	w/o	w/	w/o	w/	w/o
AUC ↑	81.22	77.15	72.43	72.41	73.63	71.47
ACC ↑	71.25	64.28	70.68	68.34	63.51	60.65
AP ↑	86.93	76.60	82.95	75.81	74.85	73.12
EER ↓	24.85	34.24	26.62	37.22	27.85	26.87

As shown in Table 4, Direct LFAD demonstrates that most of the semantic information in the cover, rather than the secret, is distributed within the low-frequency band. As a high-pass filter, HFAD is theoretically capable of extracting more secret information. The performance gap between HFAD and StegaFFD indicates that SFDA is more effective in extracting secret information. This may be attributed to HFAD’s high-pass filtering discarding excessive information, whereas differential attention adaptively suppresses interfering information, achieving greater stability. Furthermore, SFDA w/o DWT suggests that the discrete wavelet transformation contributes to more comprehensive extraction of frequency information from the stego image x_{stego} .

Effectiveness of SDA. Table 5 presents an ablation study on different loss formulations for SDA. The alignment information is categorized into Attention Alignment (AA) and Feature Alignment (FA). Based on the loss type, these are further divided into L2 loss and SDA loss, resulting in five comparative groups. The “None” group indicates the absence of any alignment loss. The combination of FA(L2)+AA(SDA) corresponds to the loss formulation used in StegaFFD. To provide a more comprehensive evaluation, we report the metrics of AUC, ACC, AP, and EER. The results demonstrate that SDA effectively assists the StegaFFD network in extracting more facial information, thereby improving FFD performance.

Effectiveness of LoD. Table 6 validates the comparison between configurations with and without LoD. To provide a more comprehensive evaluation, we report the metrics of AUC, ACC, AP, and EER. Experiments were conducted on the CDFv1, CDFv2, and UADFV datasets to ensure thorough testing. The results demonstrate that LoD enables the features extracted by SFDA to align more effectively with facial-related information, while better preserving the classification information extracted by LFAD and SFDA networks, without leading to performance degradation. Ultimately, this enhances detection accuracy.

Additionally, to demonstrate that the HiDDeN+StegaFFD combination is optimal, we compared the performance of different DIH networks in Table 7. The results show that the HiDDeN+StegaFFD combination outperforms others on most datasets.

Table 7 Performance comparison of DIH networks across datasets using AUC and EER Metrics. All metrics in the table are presented as percentages.

DIH Network	CDFv1		CDFv2		UADFV	
	AUC ↑	EER ↓	AUC ↑	EER ↓	AUC ↑	EER ↓
HiNet [122]	75.88	30.34	63.22	40.58	75.49	25.15
BalujaNet [121]	66.61	38.07	66.92	38.04	69.54	31.67
WengNet [119]	72.56	34.49	66.19	38.96	65.00	37.23
HiDDeN [120]	81.22	24.85	72.43	26.62	73.63	27.85

5 Conclusion

In this paper, we introduced StegaFFD, a novel privacy-preserving framework for Face Forgery Detection (FFD) that leverages fine-grained steganographic domain analysis. By embedding facial images within natural cover images, StegaFFD ensures covert transmission and analysis, significantly reducing the risk of arousing suspicion from attackers compared to existing privacy-enhancing methods. Our proposed Low-Frequency-Aware Decomposition (LFAD) and Spatial-Frequency Differential Attention (SFDA) modules enable effective feature lifting in the steganographic domain, mitigating interference from cover image semantics. Additionally, the Steganographic Domain Alignment (SDA) enhances detection accuracy by aligning steganographic features with facial information during training. Extensive experiments across seven facial datasets demonstrate that StegaFFD achieves state-of-the-art FFD performance and superior imperceptibility, with only a marginal performance gap compared to non-privacy-preserving methods. However, limitations remain, including slight visual artifacts in stego images and minor performance degradation due to steganographic distortions. Future work will focus on improving imperceptibility by eliminating artifacts and exploring near-lossless FFD frameworks to further bridge the performance gap, enhancing the practicality and robustness of privacy-preserving face forgery detection. StegaFFD paves the way for secure, covert facial analysis in real-world applications.

Acknowledgments

This work was supported in part by the National Natural Science Foundation of China (Nos. 62202027 and 62406320), the Strategic Priority Research Program of the Chinese Academy of Sciences (CAS)(XDB1010302), CAS Project for Young Scientists in Basic Research, Grant No. YSBR-041 and the International Partnership Program of the Chinese Academy of Sciences (CAS) (173211KYSB20200021).

Declarations of Conflict of Interest

The authors declared that they have no conflicts of interest to this work.

References

- [1] Thies, J., Zollhofer, M., Stamminger, M., Theobalt, C., Nießner, M.: Face2face: Real-time face capture and reenactment of rgb videos. In: Proceedings of the IEEE Conference on Computer Vision and Pattern Recognition, pp. 2387–2395 (2016)
- [2] Lin, X., Liu, A., Yu, Z., Cai, R., Wang, S., Yu, Y., Wan, J., Lei, Z., Cao, X., Kot, A.: Reliable and balanced transfer learning for generalized multimodal face anti-spoofing. *IEEE Transactions on Pattern Analysis and Machine Intelligence*, 1–18 (2025)
- [3] Lin, X., Wang, S., Cai, R., Liu, Y., Fu, Y., Tang, W., Yu, Z., Kot, A.C.: Suppress and rebalance: Towards generalized multi-modal face anti-spoofing. In: Proceedings of the IEEE/CVF Conference on Computer Vision and Pattern Recognition, pp. 211–221 (2024)
- [4] Cai, R., Cui, Y., Yu, Z., Lin, X., Chen, C., Kot, A.: Rehearsal-free and efficient continual learning for cross-domain face anti-spoofing. *IEEE Transactions on Pattern Analysis and Machine Intelligence*, 1–18 (2025)
- [5] Li, M., Cheung, Y.-m.: Identity-preserved complete face recovering network for partial face image. *IEEE Transactions on Emerging Topics in Computational Intelligence* **7**(2), 604–609 (2021)
- [6] Lin, X., Tang, W., Wang, H., Liu, Y., Ju, Y., Wang, S., Yu, Z.: Exposing image splicing traces in scientific publications via uncertainty-guided refinement. *Patterns* **5**(9), 101038 (2024)
- [7] Lin, X., Wang, S., Deng, J., Fu, Y., Bai, X., Chen, X., Qu, X., Tang, W.: Image manipulation detection by multiple tampering traces and edge artifact enhancement. *Pattern Recognition* **133**, 109026 (2023)
- [8] Wang, H., Deng, J., Lin, X., Tang, W., Wang, S.: Cds-net: Cooperative dual-stream network for image manipulation detection. *Pattern Recognition Letters* **176**, 167–173 (2023)
- [9] Luo, A., Kong, C., Huang, J., Hu, Y., Kang, X., Kot, A.C.: Beyond the prior forgery knowledge: Mining critical clues for general face forgery detection. *IEEE Transactions on Information Forensics and Security* **19**, 1168–1182 (2024)
- [10] Luo, A., Cai, R., Kong, C., Ju, Y., Kang, X., Huang, J., Kot, A.C.: Forgery-aware adaptive learning with vision transformer for generalized face forgery detection. *IEEE Transactions on Circuits and Systems for Video Technology* **35**(5), 4116–4129 (2025)

- [11] Kong, C., Chen, B., Li, H., Wang, S., Rocha, A., Kwong, S.: Detect and locate: Exposing face manipulation by semantic- and noise-level telltales. *IEEE Transactions on Information Forensics and Security* **17**, 1741–1756 (2022)
- [12] Kong, C., Luo, A., Xia, S., Yu, Y., Li, H., Kot, A.C.: Moe-ffd: Mixture of experts for generalized and parameter-efficient face forgery detection. *arXiv abs/2404.08452* (2024)
- [13] Lai, Y., Yu, Z., Yang, J., Li, B., Kang, X., Shen, L.: GM-DF: Generalized multi-scenario deepfake detection. In: *Proceedings of the ACM International Conference on Multimedia* (2025)
- [14] Yang, X., Li, Y., Qi, H., Lyu, S.: Exposing gan-synthesized faces using landmark locations. In: *Proceedings of the ACM Workshop on Information Hiding and Multimedia Security*, pp. 113–118 (2019)
- [15] Nataraj, L., Mohammed, T.M., Manjunath, B., Chandrasekaran, S., Flenner, A., Bappy, J.H., Roy-Chowdhury, A.K.: Detecting gan generated fake images using co-occurrence matrices. *Electronic Imaging* **31**(5) (2019)
- [16] Lin, H., Huang, W., Luo, W., Lu, W.: Deepfake detection with multi-scale convolution and vision transformer. *Digital Signal Processing* **134**, 103895 (2023)
- [17] Ma, G., Wang, Z., Yuan, X., Zhou, F.: Improving model-based deep reinforcement learning with learning degree networks and its application in robot control. *Journal of Robotics* **2022**(1), 7169594 (2022)
- [18] Ma, G., Bai, Y., Zhang, W., Yao, T., Shihada, B., Mei, T.: Boosting generic visual-linguistic representation with dynamic contexts. *IEEE Transactions on Multimedia* **25**, 8445–8457 (2023)
- [19] Meng, R., Yi, C., Yu, Y., Yang, S., Shen, B., Kot, A.C.: Semantic deep hiding for robust unlearnable examples. *IEEE Transactions on Information Forensics and Security* (2024)
- [20] Yu, Y., Yang, W., Tan, Y.-P., Kot, A.C.: Towards robust rain removal against adversarial attacks: A comprehensive benchmark analysis and beyond. In: *Proc. IEEE Int’l Conf. Computer Vision and Pattern Recognition*, pp. 6013–6022 (2022)
- [21] Yu, Y., Wang, Y., Yang, W., Lu, S., Tan, Y.-P., Kot, A.C.: Backdoor attacks against deep image compression via adaptive frequency trigger. In: *Proc. IEEE Int’l Conf. Computer Vision and Pattern Recognition*, pp. 12250–12259 (2023)

- [22] Yu, Y., Wang, Y., Xia, S., Yang, W., Lu, S., Tan, Y.-P., Kot, A.C.: Purify unlearnable examples via rate-constrained variational autoencoders. In: International Conference on Machine Learning, ICML 2024 (2024)
- [23] Yu, Y., Wang, Y., Yang, W., Guo, L., Lu, S., Duan, L.-Y., Tan, Y.-P., Kot, A.C.: Robust and transferable backdoor attacks against deep image compression with selective frequency prior. *IEEE Trans. on Pattern Analysis and Machine Intelligence* (2024)
- [24] Yu, Y., Xia, S., Lin, X., Yang, W., Lu, S., Tan, Y.-P., Kot, A.: Backdoor attacks against no-reference image quality assessment models via a scalable trigger. In: Proc. AAAI Conf. on Artificial Intelligence, vol. 39, pp. 9698–9706 (2025)
- [25] Yu, Y., Xia, S., Lin, X., Kong, C., Yang, W., Lu, S., Tan, Y.-P., Kot, A.C.: Towards model resistant to transferable adversarial examples via trigger activation. *IEEE Transactions on Information Forensics and Security* (2025)
- [26] Yu, Y., Xia, S., Yang, S., Kong, C., Yang, W., Lu, S., Tan, Y.-P., Kot, A.: Mtl-ue: Learning to learn nothing for multi-task learning. In: International Conference on Machine Learning (2025). PMLR
- [27] Wu, Q., Yu, Y., Kong, C., Liu, Z., Wan, J., Li, H., Kot, A.C., Chan, A.B.: Temporal unlearnable examples: Preventing personal video data from unauthorized exploitation by object tracking. *arXiv preprint arXiv:2507.07483* (2025)
- [28] Luo, E., Bhuiyan, M.Z.A., Wang, G., Rahman, M.A., Wu, J., Atiquzzaman, M.: Privacyprotector: Privacy-protected patient data collection in iot-based healthcare systems. *IEEE Communications Magazine* **56**(2), 163–168 (2018)
- [29] Kaissis, G.A., Makowski, M.R., Rückert, D., Braren, R.F.: Secure, privacy-preserving and federated machine learning in medical imaging. *Nature Machine Intelligence* **2**(6), 305–311 (2020)
- [30] Bagai, R., Malik, N., Jadhwal, M.: Measuring anonymity of pseudonymized data after probabilistic background attacks. *IEEE Transactions on Information Forensics and Security* **12**(5), 1156–1169 (2017)
- [31] Kaissis, G., Ziller, A., Passerat-Palmbach, J., Ryffel, T., Usynin, D., Trask, A., Lima Jr, I., Mancuso, J., Jungmann, F., Steinborn, M.-M., *et al.*: End-to-end privacy preserving deep learning on multi-institutional medical imaging. *Nature Machine Intelligence* **3**(6), 473–484 (2021)
- [32] Avudaiappan, T., Balasubramanian, R., Pandiyani, S.S., Saravanan, M.,

- Lakshmanaprabu, S., Shankar, K.: Medical image security using dual encryption with oppositional based optimization algorithm. *Journal of Medical Systems* **42**, 1–11 (2018)
- [33] Kim, B.N., Dolz, J., Desrosiers, C., Jodoin, P.: Privacy preserving for medical image analysis via non-linear deformation proxy. In: *British Machine Vision Conference*, p. 375 (2021)
- [34] Li, J., Han, L., Zhang, H., Han, X., Ge, J., Cao, X.: Learning disentangled representations for identity preserving surveillance face camouflage. In: *Proceedings of the International Conference on Pattern Recognition*, pp. 9748–9755 (2021)
- [35] Guan, H., Yap, P.-T., Bozoki, A., Liu, M.: Federated learning for medical image analysis: A survey. *Pattern Recognition*, 110424 (2024)
- [36] Liu, Y., Jia, Z., Jiang, Z., Lin, X., Liu, J., Wu, Q., Susilo, W.: Bf-sa: Blockchain-based federated learning via enhanced secure aggregation. *Journal of Systems Architecture* **152**, 103163 (2024)
- [37] Gaudio, A., Smailagic, A., Faloutsos, C., Mohan, S., Johnson, E., Liu, Y., Costa, P., Campilho, A.: *DeepFixCX*: Explainable privacy-preserving image compression for medical image analysis. *WIREs Data Mining and Knowledge Discovery* **13**(4) (2023)
- [38] Packhäuser, K., Gündel, S., Thamm, F., Denzinger, F., Maier, A.K.: Deep learning-based anonymization of chest radiographs: A utility-preserving measure for patient privacy. In: *Medical Image Computing and Computer Assisted Intervention*, vol. 14222, pp. 262–272 (2023)
- [39] Kim, B.N., Dolz, J., Jodoin, P., Desrosiers, C.: Privacy-net: An adversarial approach for identity-obfuscated segmentation of medical images. *IEEE Trans. Medical Imaging* **40**(7), 1737–1749 (2021)
- [40] Shiri, I., Razeghi, B., Ferdowsi, S., Salimi, Y., Gündüz, D., Teodoro, D., Voloshynovskiy, S., Zaidi, H.: Primis: Privacy-preserving medical image sharing via deep sparsifying transform learning with obfuscation. *Journal of Biomedical Informatics* **150**, 104583 (2024)
- [41] Yang, Z., Chen, Y., Huangfu, H., Ran, M., Wang, H., Li, X., Zhang, Y.: Dynamic corrected split federated learning with homomorphic encryption for u-shaped medical image networks. *IEEE Journal of Biomedical and Health Informatics* **27**(12), 5946–5957 (2023)
- [42] Zhu, D., Zhu, H., Huang, C., Lu, R., Feng, D., Shen, X.: Efficient and accurate cloud-assisted medical pre-diagnosis with privacy preservation. *IEEE Trans. Dependable Secur. Comput.* **21**(2), 860–875 (2024)

- [43] Guan, Z., Jing, J., Deng, X., Xu, M., Jiang, L., Zhang, Z., Li, Y.: Deepmih: Deep invertible network for multiple image hiding. *IEEE Trans. Pattern Anal. Mach. Intell.* **45**(1), 372–390 (2022)
- [44] Jing, J., Deng, X., Xu, M., Wang, J., Guan, Z.: Hinet: Deep image hiding by invertible network. In: *International Conference on Computer Vision*, pp. 4733–4742 (2021)
- [45] Li, G., Li, S., Luo, Z., Qian, Z., Zhang, X.: Purified and unified steganographic network. In: *IEEE Conference on Computer Vision and Pattern Recognition* (2024)
- [46] Lin, X., Yu, Y., Yu, Z., Meng, R., Zhou, J., Liu, A., Liu, Y., Wang, S., Tang, W., Lei, Z., Kot, A.C.: HideMIA: Hidden wavelet mining for privacy-enhancing medical image analysis. In: *Proceedings of the ACM International Conference on Multimedia*, pp. 8110–8119 (2024)
- [47] Deng, X., Gao, C., Xu, M.: Pirnet: Privacy-preserving image restoration network via wavelet lifting. In: *Proceedings of the IEEE/CVF International Conference on Computer Vision*, pp. 22311–22320 (2023)
- [48] Chen, L., Fu, Y., Gu, L., Yan, C., Harada, T., Huang, G.: Frequency-aware feature fusion for dense image prediction. *IEEE Transactions on Pattern Analysis and Machine Intelligence* (2024)
- [49] Chen, L., Gu, L., Zheng, D., Fu, Y.: Frequency-adaptive dilated convolution for semantic segmentation. In: *Proceedings of the IEEE/CVF Conference on Computer Vision and Pattern Recognition*, pp. 3414–3425 (2024)
- [50] Yang, L., Zhang, R.-Y., Li, L., Xie, X.: Simam: A simple, parameter-free attention module for convolutional neural networks. In: *International Conference on Machine Learning*, pp. 11863–11874 (2021)
- [51] Li, Z., Xu, P., Chang, X., Yang, L., Zhang, Y., Yao, L., Chen, X.: When object detection meets knowledge distillation: A survey. *IEEE Transactions on Pattern Analysis and Machine Intelligence* **45**(8), 10555–10579 (2023)
- [52] Sadeghi, A.-R., Schneider, T., Wehrenberg, I.: Efficient privacy-preserving face recognition. In: *International Conference on Information Security and Cryptology*, pp. 229–244 (2009)
- [53] Huang, Y., Song, Z., Li, K., Arora, S.: Instahide: Instance-hiding schemes for private distributed learning. In: *International Conference on Machine Learning*, pp. 4507–4518 (2020)

- [54] Ma, Z., Liu, Y., Liu, X., Ma, J., Ren, K.: Lightweight privacy-preserving ensemble classification for face recognition. *IEEE Internet of Things Journal* **6**(3), 5778–5790 (2019)
- [55] Wang, Y., Liu, J., Luo, M., Yang, L., Wang, L.: Privacy-preserving face recognition in the frequency domain. In: *Proceedings of the AAAI Conference on Artificial Intelligence*, vol. 36, pp. 2558–2566 (2022)
- [56] Li, Y., Wang, Y., Li, D.: Privacy-preserving lightweight face recognition. *Neurocomputing* **363**, 212–222 (2019)
- [57] Ergun, O.O.: Privacy preserving face recognition in encrypted domain. In: *IEEE Asia Pacific Conference on Circuits and Systems*, pp. 643–646 (2014)
- [58] Winkler, T., Rinner, B.: Trustcam: Security and privacy-protection for an embedded smart camera based on trusted computing. In: *IEEE International Conference on Advanced Video and Signal Based Surveillance*, pp. 593–600 (2010)
- [59] Hukkelås, H., Mester, R., Lindseth, F.: Deepprivacy: A generative adversarial network for face anonymization. In: *International Symposium on Visual Computing*, pp. 565–578 (2019)
- [60] Zhao, J., Xiong, L., Karlekar Jayashree, P., Li, J., Zhao, F., Wang, Z., Sugiri Pranata, P., Shengmei Shen, P., Yan, S., Feng, J.: Dual-agent gans for photorealistic and identity preserving profile face synthesis. *Advances in Neural Information Processing Systems* **30** (2017)
- [61] Yuan, L., Liu, L., Pu, X., Li, Z., Li, H., Gao, X.: Pro-face: A generic framework for privacy-preserving recognizable obfuscation of face images. In: *Proceedings of the ACM International Conference on Multimedia*, pp. 1661–1669 (2022)
- [62] Zhang, Y., Wang, T., Zhao, R., Wen, W., Zhu, Y.: Rapp: Reversible privacy preservation for various face attributes. *IEEE Transactions on Information Forensics and Security* **18**, 3074–3087 (2023)
- [63] Wang, T., Zhang, Y., Zhao, R., Wen, W., Lan, R.: Identifiable face privacy protection via virtual identity transformation. *IEEE Signal Processing Letters* **30**, 773–777 (2023)
- [64] Baluja, S.: Hiding images in plain sight: Deep steganography. *Advances in Neural Information Processing Systems*, 2069–2079 (2017)
- [65] Hayes, J., Danezis, G.: Generating steganographic images via adversarial training. In: *Advances in Neural Information Processing Systems*, pp.

1954–1963 (2017)

- [66] Liu, L., Meng, L., Peng, Y., Wang, X.: A data hiding scheme based on u-net and wavelet transform. *Knowledge-Based Systems* **223**, 107022 (2021)
- [67] He, Z., Lu, W., Sun, W., Huang, J.: Digital image splicing detection based on markov features in DCT and DWT domain. *Pattern Recognition* **45**(12), 4292–4299 (2012)
- [68] Xiao, M., Zheng, S., Liu, C., Wang, Y., He, D., Ke, G., Bian, J., Lin, Z., Liu, T.-Y.: Invertible image rescaling. In: *European Conference on Computer Vision*, pp. 126–144 (2020)
- [69] Xing, Y., Qian, Z., Chen, Q.: Invertible image signal processing. In: *IEEE Conference on Computer Vision and Pattern Recognition*, pp. 6287–6296 (2021)
- [70] Lu, S., Wang, R., Zhong, T., Rosin, P.L.: Large-capacity image steganography based on invertible neural networks. In: *IEEE Conference on Computer Vision and Pattern Recognition*, pp. 10816–10825 (2021)
- [71] Zhang, Y., Zheng, L., Thing, V.L.: Automated face swapping and its detection. In: *Proceedings of the IEEE International Conference on Signal and Image Processing*, pp. 15–19 (2017)
- [72] Koopman, M., Rodriguez, A.M., Geradts, Z.: Detection of deepfake video manipulation. In: *Proceedings of the Irish Machine Vision and Image Processing Conference*, pp. 133–136 (2018)
- [73] Afchar, D., Nozick, V., Yamagishi, J., Echizen, I.: Mesonet: a compact facial video forgery detection network. In: *IEEE International Workshop on Information Forensics and Security*, pp. 1–7 (2018)
- [74] Rossler, A., Cozzolino, D., Verdoliva, L., Riess, C., Thies, J., Nießner, M.: Faceforensics++: Learning to detect manipulated facial images. In: *Proceedings of the IEEE/CVF International Conference on Computer Vision*, pp. 1–11 (2019)
- [75] Zhang, Y., Ma, G., Hao, G., Guo, L., Chen, Y., Yu, S.: Efficient reinforcement learning through adaptively pretrained visual encoder. In: *Proceedings of the AAAI Conference on Artificial Intelligence*, vol. 39, pp. 22668–22676 (2025)
- [76] Nguyen, H.H., Fang, F., Yamagishi, J., Echizen, I.: Multi-task learning for detecting and segmenting manipulated facial images and videos. In: *Proceedings on IEEE International Conference on Biometrics Theory,*

- Applications and Systems, pp. 1–8 (2019)
- [77] Nguyen, H.H., Yamagishi, J., Echizen, I.: Capsule-forensics: Using capsule networks to detect forged images and videos. In: Proceedings of the IEEE International Conference on Acoustics, Speech, and Signal Processing, pp. 2307–2311 (2019)
- [78] Qian, Y., Yin, G., Sheng, L., Chen, Z., Shao, J.: Thinking in frequency: Face forgery detection by mining frequency-aware clues. In: Proceedings of the European Conference on Computer Vision, pp. 86–103 (2020)
- [79] Liu, H., Li, X., Zhou, W., Chen, Y., He, Y., Xue, H., Zhang, W., Yu, N.: Spatial-phase shallow learning: rethinking face forgery detection in frequency domain. In: Proceedings of the IEEE/CVF Conference on Computer Vision and Pattern Recognition, pp. 772–781 (2021)
- [80] Durall, R., Keuper, M., Keuper, J.: Watch your up-convolution: Cnn based generative deep neural networks are failing to reproduce spectral distributions. In: Proceedings of the IEEE/CVF Conference on Computer Vision and Pattern Recognition, pp. 7890–7899 (2020)
- [81] Yan, Z., Zhang, Y., Fan, Y., Wu, B.: Ucf: Uncovering common features for generalizable deepfake detection. In: Proceedings of the IEEE/CVF International Conference on Computer Vision, pp. 22412–22423 (2023)
- [82] Ma, G., Zhang, Y., Dai, Y., Hao, G., Chen, Y., Yu, S.: Clustering-based weight orthogonalization for stabilizing deep reinforcement learning. In: 2025 International Joint Conference on Neural Networks (IJCNN), pp. 1–9 (2025). IEEE
- [83] Ma, G., Zhang, Y., Dai, Y., Hao, G., Chen, Y., Yu, S.: Mitigating non-stationarity in deep reinforcement learning with clustering orthogonal weight modification. In: Proceedings of the 24th International Conference on Autonomous Agents and Multiagent Systems, pp. 2648–2650 (2025)
- [84] Cao, J., Ma, C., Yao, T., Chen, S., Ding, S., Yang, X.: End-to-end reconstruction-classification learning for face forgery detection. In: Proceedings of the IEEE/CVF Conference on Computer Vision and Pattern Recognition, pp. 4113–4122 (2022)
- [85] Wang, C., Deng, W.: Representative forgery mining for fake face detection. In: Proceedings of the IEEE/CVF Conference on Computer Vision and Pattern Recognition, pp. 14923–14932 (2021)
- [86] Li, Y., Lyu, S.: Exposing deepfake videos by detecting face warping artifacts. arXiv preprint arXiv:1811.00656 (2018)

- [87] Luo, Y., Zhang, Y., Yan, J., Liu, W.: Generalizing face forgery detection with high-frequency features. In: Proceedings of the IEEE/CVF Conference on Computer Vision and Pattern Recognition, pp. 16317–16326 (2021)
- [88] Wen, D., Han, H., Jain, A.K.: Face spoof detection with image distortion analysis. *IEEE Transactions on Information Forensics and Security* **10**(4), 746–761 (2015)
- [89] Chen, B., Liu, X., Xia, Z., Zhao, G.: Privacy-preserving deepfake face image detection. *Digital Signal Processing* **143**, 104233 (2023)
- [90] Abadi, M., Chu, A., Goodfellow, I., McMahan, H.B., Mironov, I., Talwar, K., Zhang, L.: Deep learning with differential privacy. In: Proceedings of the ACM SIGSAC Conference on Computer and Communications Security, pp. 308–318 (2016)
- [91] Luo, C., Lin, Q., Xie, W., Wu, B., Xie, J., Shen, L.: Frequency-driven imperceptible adversarial attack on semantic similarity. In: Proceedings of the IEEE/CVF Conference on Computer Vision and Pattern Recognition, pp. 15315–15324 (2022)
- [92] Lu, H., Liu, W., Fu, H., Cao, Z.: FADE: Fusing the assets of decoder and encoder for task-agnostic upsampling. In: Proceedings of the European Conference on Computer Vision, pp. 231–247 (2022)
- [93] Zou, X., Xiao, F., Yu, Z., Li, Y., Lee, Y.J.: Delving deeper into anti-aliasing in convnets. *International Journal of Computer Vision* **131**(1), 67–81 (2023)
- [94] Laplante, P.A., Cravey, R., Dunleavy, L.P., Antonakos, J.L., LeRoy, R., East, J., Buris, N.E., Conant, C.J., Fryda, L., Boyd, R.W., *et al.*: *Comprehensive Dictionary of Electrical Engineering*, (2018)
- [95] Vaswani, A., Shazeer, N., Parmar, N., Uszkoreit, J., Jones, L., Gomez, A.N., Kaiser, L., Polosukhin, I.: Attention is all you need. *Advances in Neural Information Processing Systems* **30** (2017)
- [96] Guo, X., Tang, W., Wang, H., Wang, J., Wang, S., Qu, X., Lin, X.: MorFormer: morphology-aware transformer for generalized pavement crack segmentation. *IEEE Transactions on Intelligent Transportation Systems* **26**(6), 8219–8232 (2025)
- [97] Hao, G., Zhang, Y., Ma, G., Chen, Y., Alexandre, F., Yu, S.: Position paper: Large language models need episodic memory. In: 2025 International Joint Conference on Neural Networks (IJCNN), pp. 1–10 (2025). IEEE

- [98] Zhang, B., Sennrich, R.: Root mean square layer normalization. *Advances in Neural Information Processing Systems* **32**, 12360–12371 (2019)
- [99] Touvron, H., Lavril, T., Izacard, G., Martinet, X., Lachaux, M.-A., Lacroix, T., Rozière, B., Goyal, N., Hambro, E., Azhar, F., et al.: Llama: Open and efficient foundation language models. *arXiv preprint arXiv:2302.13971* (2023)
- [100] Wu, Y., He, K.: Group normalization. In: *Proceedings of the European Conference on Computer Vision*, pp. 3–19 (2018)
- [101] Wang, H., Ma, S., Huang, S., Dong, L., Wang, W., Peng, Z., Wu, Y., Bajaj, P., Singhal, S., Benhaim, A., et al.: Magneto: A foundation transformer. In: *International Conference on Machine Learning*, pp. 36077–36092 (2023)
- [102] Qin, Z., Han, X., Sun, W., Li, D., Kong, L., Barnes, N., Zhong, Y.: The devil in linear transformer. *arXiv preprint arXiv:2210.10340* (2022)
- [103] Ma, G.: Decoupled planning and execution with llm-driven world models for efficient reinforcement learning. In: *NeurIPS 2025 Workshop on Embodied World Models for Decision Making*
- [104] Gretton, A., Borgwardt, K.M., Rasch, M.J., Schölkopf, B., Smola, A.: A kernel two-sample test. *The Journal of Machine Learning Research* **13**(1), 723–773 (2012)
- [105] Sun, B., Saenko, K.: Deep coral: Correlation alignment for deep domain adaptation. In: *Proceedings of the European Conference on Computer Vision Workshops*, pp. 443–450 (2016)
- [106] Chen, C., Fu, Z., Chen, Z., Jin, S., Cheng, Z., Jin, X., Hua, X.-S.: Homm: Higher-order moment matching for unsupervised domain adaptation. In: *Proceedings of the AAAI Conference on Artificial Intelligence*, vol. 34, pp. 3422–3429 (2020)
- [107] Pérez-Cruz, F.: Kullback-leibler divergence estimation of continuous distributions. In: *IEEE International Symposium on Information Theory*, pp. 1666–1670 (2008)
- [108] Jose, S.T., Simeone, O.: Information-theoretic bounds on transfer generalization gap based on jensen-shannon divergence. In: *European Signal Processing Conference*, pp. 1461–1465 (2021)
- [109] Rüschemdorf, L.: The wasserstein distance and approximation theorems. *Probability Theory and Related Fields* **70**(1), 117–129 (1985)

- [110] Xue, Y., Wu, J., Ji, R., Zhong, P., Wen, J., Peng, W.: Adaptive domain-invariant feature extraction for cross-domain linguistic steganalysis. *IEEE Transactions on Information Forensics and Security* **19**, 920–933 (2023)
- [111] Ye, T., Dong, L., Xia, Y., Sun, Y., Zhu, Y., Huang, G., Wei, F.: Differential transformer. In: *Proceedings of International Conference on Learning Representations* (2025)
- [112] Li, Y., Yang, X., Sun, P., Qi, H., Lyu, S.: Celeb-df: A large-scale challenging dataset for deepfake forensics. In: *Proceedings of the IEEE/CVF Conference on Computer Vision and Pattern Recognition*, pp. 3207–3216 (2020)
- [113] Rana, M.S., Nobi, M.N., Murali, B., Sung, A.H.: Deepfake detection: A systematic literature review. *IEEE Access* **10**, 25494–25513 (2022)
- [114] Dolhansky, B., Howes, R., Pflaum, B., Baram, N., Ferrer, C.C.: The deepfake detection challenge (dfdc) preview dataset. *arXiv preprint arXiv:1910.08854* (2019)
- [115] Dolhansky, B., Bitton, J., Pflaum, B., Lu, J., Howes, R., Wang, M., Ferrer, C.C.: The deepfake detection challenge (dfdc) dataset. *arXiv preprint arXiv:2006.07397* (2020)
- [116] Li, Y., Chang, M.-C., Lyu, S.: In ictu oculi: Exposing ai created fake videos by detecting eye blinking. In: *IEEE International Workshop on Information Forensics and Security*, pp. 1–7 (2018)
- [117] Li, L., Bao, J., Yang, H., Chen, D., Wen, F.: Advancing high fidelity identity swapping for forgery detection. In: *Proceedings of the IEEE/CVF Conference on Computer Vision and Pattern Recognition*, pp. 5074–5083 (2020)
- [118] Barattin, S., Tzelepis, C., Patras, I., Sebe, N.: Attribute-preserving face dataset anonymization via latent code optimization. In: *Proceedings of the IEEE/CVF Conference on Computer Vision and Pattern Recognition*, pp. 8001–8010 (2023)
- [119] Weng, X., Li, Y., Chi, L., Mu, Y.: High-capacity convolutional video steganography with temporal residual modeling. In: *Proceedings of the International Conference on Multimedia Retrieval*, pp. 87–95 (2019)
- [120] Zhu, J., Kaplan, R., Johnson, J., Fei-Fei, L.: Hidden: Hiding data with deep networks. In: *Proceedings of the European Conference on Computer Vision*, pp. 657–672 (2018)

- [121] Baluja, S.: Hiding images within images. *IEEE Transactions on Pattern Analysis and Machine Intelligence* **42**(7), 1685–1697 (2019)
- [122] Jing, J., Deng, X., Xu, M., Wang, J., Guan, Z.: Hinet: Deep image hiding by invertible network. In: *Proceedings of the IEEE/CVF International Conference on Computer Vision*, pp. 4733–4742 (2021)
- [123] Sagonas, C., Antonakos, E., Tzimiropoulos, G., Zafeiriou, S., Pantic, M.: 300 faces in-the-wild challenge: Database and results. *Image and Vision Computing* **47**, 3–18 (2016)
- [124] Selvaraju, R.R., Cogswell, M., Das, A., Vedantam, R., Parikh, D., Batra, D.: Grad-cam: Visual explanations from deep networks via gradient-based localization. *International Journal of Computer Vision* **128**(2), 336–359 (2020)